



## Examining Rapid Onset Drought Development Using the Thermal Infrared–Based Evaporative Stress Index

JASON A. OTKIN,<sup>\*</sup> MARTHA C. ANDERSON,<sup>+</sup> CHRISTOPHER HAIN,<sup>#</sup> ILIANA E. MLADENOVA,<sup>+</sup>  
JEFFREY B. BASARA,<sup>@</sup> AND MARK SVOBODA<sup>&</sup>

<sup>\*</sup> *Cooperative Institute for Meteorological Satellite Studies, University of Wisconsin—Madison, Madison, Wisconsin*

<sup>+</sup> *Agricultural Research Services, United States Department of Agriculture, Hydrology and Remote Sensing Laboratory, Beltsville, Maryland*

<sup>#</sup> *Earth System Interdisciplinary Center, University of Maryland, College Park, College Park, Maryland*

<sup>@</sup> *School of Meteorology, and Oklahoma Climatological Survey, University of Oklahoma, Norman, Oklahoma*

<sup>&</sup> *National Drought Mitigation Center, University of Nebraska–Lincoln, Lincoln, Nebraska*

(Manuscript received 2 October 2012, in final form 11 April 2013)

### ABSTRACT

Reliable indicators of rapid drought onset can help to improve the effectiveness of drought early warning systems. In this study, the evaporative stress index (ESI), which uses remotely sensed thermal infrared imagery to estimate evapotranspiration (ET), is compared to drought classifications in the U.S. Drought Monitor (USDM) and standard precipitation-based drought indicators for several cases of rapid drought development that have occurred across the United States in recent years. Analysis of meteorological time series from the North American Regional Reanalysis indicates that these events are typically characterized by warm air temperature and low cloud cover anomalies, often with high winds and dewpoint depressions that serve to hasten evaporative depletion of soil moisture reserves. Standardized change anomalies depicting the rate at which various multiweek ESI composites changed over different time intervals are computed to more easily identify areas experiencing rapid changes in ET. Overall, the results demonstrate that ESI change anomalies can provide early warning of incipient drought impacts on agricultural systems, as indicated in crop condition reports collected by the National Agricultural Statistics Service. In each case examined, large negative change anomalies indicative of rapidly drying conditions were either coincident with the introduction of drought in the USDM or lead the USDM drought depiction by several weeks, depending on which ESI composite and time-differencing interval was used. Incorporation of the ESI as a data layer used in the construction of the USDM may improve timely depictions of moisture conditions and vegetation stress associated with flash drought events.

### 1. Introduction

Drought conditions can adversely affect the health of native vegetation and agricultural crops if the abnormal dryness persists for an extended period of time or if it occurs at a sensitive stage of crop development. Non-irrigated agricultural lands are especially vulnerable to drought on both short and long time scales because they depend on receiving adequate rainfall throughout the

growing season (Kogan 1997). Depending on its severity and timing, drought can result in significant yield loss, with impacts on both local and global economies signified through reduced economic output and higher grain and food prices. Long-term drought may lead to lower reservoir levels and depleted groundwater levels that could also limit the productivity of irrigated cropland because of water shortages and smaller water allocations.

Although drought is often thought of as a slowly developing climate phenomenon that can take several months or even years to reach its maximum intensity, drought onset can be very rapid if extreme atmospheric

---

*Corresponding author address:* Jason A. Otkin, 1225 W. Dayton St., Madison, WI 53706.  
E-mail: jason.otkin@ssec.wisc.edu

anomalies persist for several weeks. Vegetation health can deteriorate very quickly during an extended period of dry weather if the lack of rainfall is also accompanied by anomalously warm surface temperatures, strong winds, and sunny skies because these conditions lead to increased evapotranspiration (ET) that can quickly deplete root zone moisture (Mozny et al. 2012). This scenario is most likely to occur during the warm season when daily mean temperatures and potential evaporation tend to be highest. In recent years, the term “flash drought” has been used to describe these events to better distinguish them from more slowly evolving droughts (Svoboda et al. 2002). Because flash droughts are more likely to occur during the growing season, agricultural crops tend to suffer the greatest impacts. Even short periods of intense water stress can lead to significant yield loss and reduced grain quality if they occur during sensitive stages in crop development such as emergence, pollination, and grain filling (e.g., Barnabás et al. 2008; Rötter and van de Geijn 1999; Saini and Westgate 1999; Li et al. 2009; Mishra and Cherkauer 2010; Mkhabela et al. 2010; Prasad et al. 2011; Swain et al. 2011; Pradhan et al. 2012). The simultaneous occurrence of depleted soil moisture and heat stress has an even larger detrimental effect on plant growth, reproduction, and yield than when either of these stresses occurs individually (Jiang and Huang 2001; Rizhsky et al. 2002; Ciais et al. 2005; Mittler 2006; Prasad et al. 2011; Kebede et al. 2012).

Flash droughts are difficult to identify using traditional precipitation-based drought indices such as the standardized precipitation index (SPI; McKee et al. 1993, 1995) because precipitation deficits are only one factor contributing to their development. Though the SPI can be computed for shorter time periods, such as one month, to better capture short-term precipitation deficits, its utility is still limited because it does not account for temperature, wind, and radiation anomalies associated with flash drought development. Flash droughts can occur even when the SPI indicates only moderate precipitation deficits. The Palmer drought severity index (Palmer 1965) uses both precipitation and temperature observations, but it is more effective at identifying long-term drought conditions developing over a period of several months or more because the index responds slowly to changes in prevailing weather regimes (Karl 1986) and may be overly sensitive to temperature effects (Hu and Willson 2000). Drought indices based on remotely sensed observations of green biomass such as the vegetation drought response index (Brown et al. 2008) can be used to identify areas experiencing poor vegetation

health because of drought; however, vegetation indices are less able to detect incipient plant stress during early stages of drought development because the signal only becomes strong after significant damage has already occurred to the vegetation (Moran 2003).

A faster response signal of incipient drought stress may be conveyed through remotely sensed maps of land surface temperature (LST), retrieved using satellite-based thermal infrared (TIR) observations (Anderson et al. 2013). As the amount of root zone moisture decreases, less energy is used to evaporate and transpire water, thereby causing canopy temperatures to elevate in comparison with unstressed vegetation under the same atmospheric conditions. The TIR-based Atmospheric Land Exchange Inverse (ALEXI; Anderson et al. 1997; Mecikalski et al. 1999; Anderson et al. 2007b) surface energy balance model estimates actual ET at continental scales using the morning rise in remotely sensed LST. The severity of the drought stress can be inferred from anomalies in the ratio of actual to potential ET (PET), as quantified by the ALEXI-based Evaporative Stress Index (ESI; Anderson et al. 2007c, 2011, 2013). ET-based drought metrics derived from thermal remote sensing may be uniquely sensitive to rapidly changing soil moisture conditions, inherently capturing the impacts of temperature, humidity, wind, and radiation anomalies associated with flash drought development.

In this paper, we examine the characteristic evolution of meteorological conditions and ESI drought indicator response associated with several flash drought events that have impacted agricultural areas of the United States in recent years as recorded in the U.S. Drought Monitor (USDM; Svoboda et al. 2002). The goal of this study is to evaluate the potential value of including a fast-response drought indicator like the ESI within the USDM process in terms of improving early detection and to explore new drought visualization tools based on change detection. Ground-based crop condition data collected by the U.S. Department of Agriculture (USDA) National Agricultural Statistics Service (NASS) are included in the analysis to demonstrate relative timing of observed impacts on crops and rangeland within the study regions. The ability of weekly changes in multiweek ESI composites to provide early warning of worsening drought conditions will also be examined. Section 2 contains a description of the ESI, USDM, crop condition, and meteorological datasets. Case studies associated with four representative rapid onset drought events within the United States are presented in section 3, with conclusions in section 4.

## 2. Data and methodology

### a. ESI

The ESI is computed using actual ET estimates from the ALEXI model, which is run daily over the contiguous United States (CONUS) with 10-km horizontal grid spacing. ALEXI uses a two-source energy balance (TSEB) model initially developed by Norman et al. (1995) to consider energy processes for vegetated and bare soil components of the land surface. In the TSEB, LST is used to directly constrain the sensible heat flux, with the latent heat flux [ $\lambda E$  ( $\text{W m}^{-2}$ ), where  $E$  is ET ( $\text{mm s}^{-1}$  or  $\text{kg s}^{-1} \text{m}^{-2}$ ) and  $\lambda$  is the latent heat of evaporation ( $\text{J kg}^{-1}$ )] computed as a residual of the overall energy balance equation. Partitioning of LST and energy fluxes between the soil and canopy components of the land surface is informed by estimates of vegetation cover fraction or leaf area index.

ALEXI employs the TSEB in a time-differential mode, using the observed morning rise in LST, as measured with geostationary satellites from  $\sim 1.5$  h after local sunrise to 1.5 h before local noon, to infer the surface energy budget. Use of time-differential observations reduces model sensitivity to errors in absolute temperature retrievals resulting from sensor calibration and atmospheric correction. A simple model of atmospheric boundary layer (ABL) growth (McNaughton and Spriggs 1986) is used to provide closure to the time-integrated energy balance equations over the morning period, alleviating the need for specifying near-surface boundary conditions in air temperature, which often precludes regional applications of LST-based energy balance algorithms (Anderson et al. 1997).

Over CONUS, ALEXI uses LST data from the Geostationary Operational Environmental Satellites (GOES) Sounder, vegetation cover fraction derived from the 8-day Moderate Resolution Imaging Spectroradiometer (MODIS) leaf area index product (MOD15A2; Myneni et al. 2002), and hourly insolation from the GOES imager (Otkin et al. 2005). The ABL model component also uses the general slope (i.e., lapse rate) of the ABL temperature profile, which is obtained from the North American Regional Reanalysis (NARR; Mesinger et al. 2006). In comparison with tower flux measurements, typical errors in daily ET have been found to be on the order of 10%–15% of the mean observed flux for a variety of vegetation types and climate conditions (Anderson et al. 2007a, 2007b, 2012). The reader is referred to Anderson et al. (2007b) for a complete description of the ALEXI system.

To minimize the impact of non-moisture-related drivers on ET when computing the ESI, the ALEXI ET is normalized with respect to a reference flux ( $F_{\text{ref}}$ ) to

obtain an ET fraction ( $\text{ET}_{\text{ALEXI}}/F_{\text{ref}}$ ). Standardized anomalies in the ET fraction are then calculated over the ALEXI 2000–11 period of record. Anderson et al. (2013) evaluated several possible forms of scaling flux and found that the Penman–Monteith (PM) formulation for reference ET as codified in Allen et al. (1998) provided optimal spatial and temporal correlations between the ESI and other drought indicators such as the USDM and soil moisture anomalies from the North American Land Data Assimilation System (Xia et al. 2012a, 2012b). Meteorological inputs to the PM computation were obtained from the NARR dataset.

Because the ALEXI algorithm relies on the morning rise in LST to compute ET, it is only applicable to satellite pixels that remain clear during the morning interval used to compute the change in LST. A cloud mask algorithm is used to remove most cloudy pixels; however, optically thin clouds are more difficult to detect and can lead to spurious ET retrievals by changing the magnitude of the morning rise in LST used to infer the surface energy budget. Anderson et al. (2013) discusses a temporal smoothing algorithm that reduces random noise in daily ET retrievals caused by incomplete cloud screening. On average, daily ET values are computed at least once per week for 75% of the CONUS grid points, with 95% of the domain updated at least once every 20 days (Anderson et al. 2007b). More complete domain coverage can be achieved by compositing clear-sky ET estimates over longer multi-week periods.

The clear-sky composites are computed as an average of all values over a given interval that passes the cloud screening tests:

$$\langle v(w, y) \rangle = \frac{1}{\text{nc}} \sum_{n=1}^{\text{nc}} v(n, y), \quad (1)$$

where  $\langle v(w, y) \rangle$  is the composite for week  $w$  and year  $y$  at a given grid point;  $v(n, y)$  is the ET fraction on day  $n$ ; and  $\text{nc}$  is the number of clear days during the compositing interval. Although this dependence on clear-sky retrievals and temporal compositing somewhat degrades response time to changing surface moisture conditions, flash droughts are typically associated with predominantly clear skies; therefore, temporal sampling should be maximized during such events.

ESI anomalies are routinely computed over 2-, 4-, and 8-week composite periods, which advance on weekly time steps. These composites are hereafter denoted as ESI\_02WK, ESI\_04WK, and ESI\_08WK. The anomalies are expressed as pseudo  $z$  scores normalized to a mean of 0 and a standard deviation of 1. Fields describing the mean conditions and standard deviation at

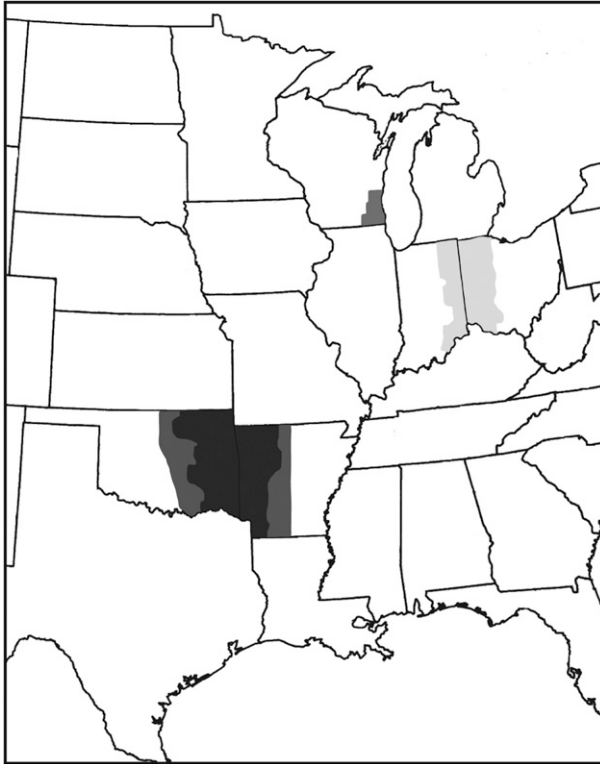


FIG. 1. Locations of the four flash drought case study areas examined in section 3. The southeast Wisconsin and Indiana–Ohio regions are denoted by the medium and light gray colors. The Oklahoma–Arkansas region examined in section 3d is denoted by the black color, whereas the larger Oklahoma–Arkansas region examined in section 3a includes the black shaded area and the surrounding dark gray region.

each grid point during the ALEXI period of record (2000–11) were generated for each composite interval.

Standardized anomalies were then computed each week at each grid point as

$$\text{ESI}(w, y) = \frac{\langle v(w, y) \rangle - \frac{1}{ny} \sum_{y=1}^{ny} \langle v(w, y) \rangle}{\sigma(w)}, \quad (2)$$

where the second term in the numerator defines the mean conditions averaged over all years and the denominator is the standard deviation. Equation (2) was modified from the original specification in Anderson et al. [2007c, their Eq. (2)], effectively absorbing the statistical normalization into the definition of ESI to simplify notation and conforming to standard sign conventions used in most drought indices. Negative values represent periods of reduced soil moisture availability or poorer-than-average vegetation health. Assuming a normal distribution, ESI values less than  $-1$  represent dry conditions exceeding  $1\sigma$ , which should occur  $\sim 16\%$  of the time. There are currently too few years in the ALEXI archive to warrant using a nonnormal distribution; however, such methods may be applied as the archive length continues to increase.

Temporal changes in the ESI composites may convey useful information about the rate at which vegetation conditions are deteriorating during the early stages of drought development. To facilitate identification of areas of significant change at different time scales, standardized ESI change anomalies were computed for composites separated by 1-, 2-, 3-, and 4-week change intervals. These standardized change variables (denoted  $\Delta\text{ESI}$ ) were generated by differencing composites of smoothed  $\text{ET}/F_{\text{ref}}$ , then computing standardized anomalies in the difference products using Eq. (3):

$$\Delta\text{ESI}(w_1, w_2, y) = \frac{\langle v(w_2, y) - v(w_1, y) \rangle - \frac{1}{ny} \sum_{y=1}^{ny} \langle v(w_2, y) - v(w_1, y) \rangle}{\sigma(w_1, w_2)} \quad (3)$$

where  $w_1$  and  $w_2$  are the two weeks used in the difference computation. This final step is valuable (in comparison with delivering simple time differences between ESI products) because it brings maps at all change intervals to a common magnitude scale and highlights the significance of change in comparison with climatology. Standardized change anomalies were generated for each of the ESI composite periods (2, 4, and 8 weeks). As will be shown in section 3, the resultant suite of 12 ESI change variables can in some cases provide early

warning of impending drought conditions across multiple time scales. Large negative change anomalies indicate that water stress is increasing rapidly relative to average conditions experienced during the 12-yr ALEXI climatology. ESI and  $\Delta\text{ESI}$  maps at 10-km resolution are distributed in real time during the nominal growing season (April–October; <http://hrs.arsusda.gov/drought>) and through the National Integrated Drought Information Service (NIDIS) portal ([www.drought.gov](http://www.drought.gov)).

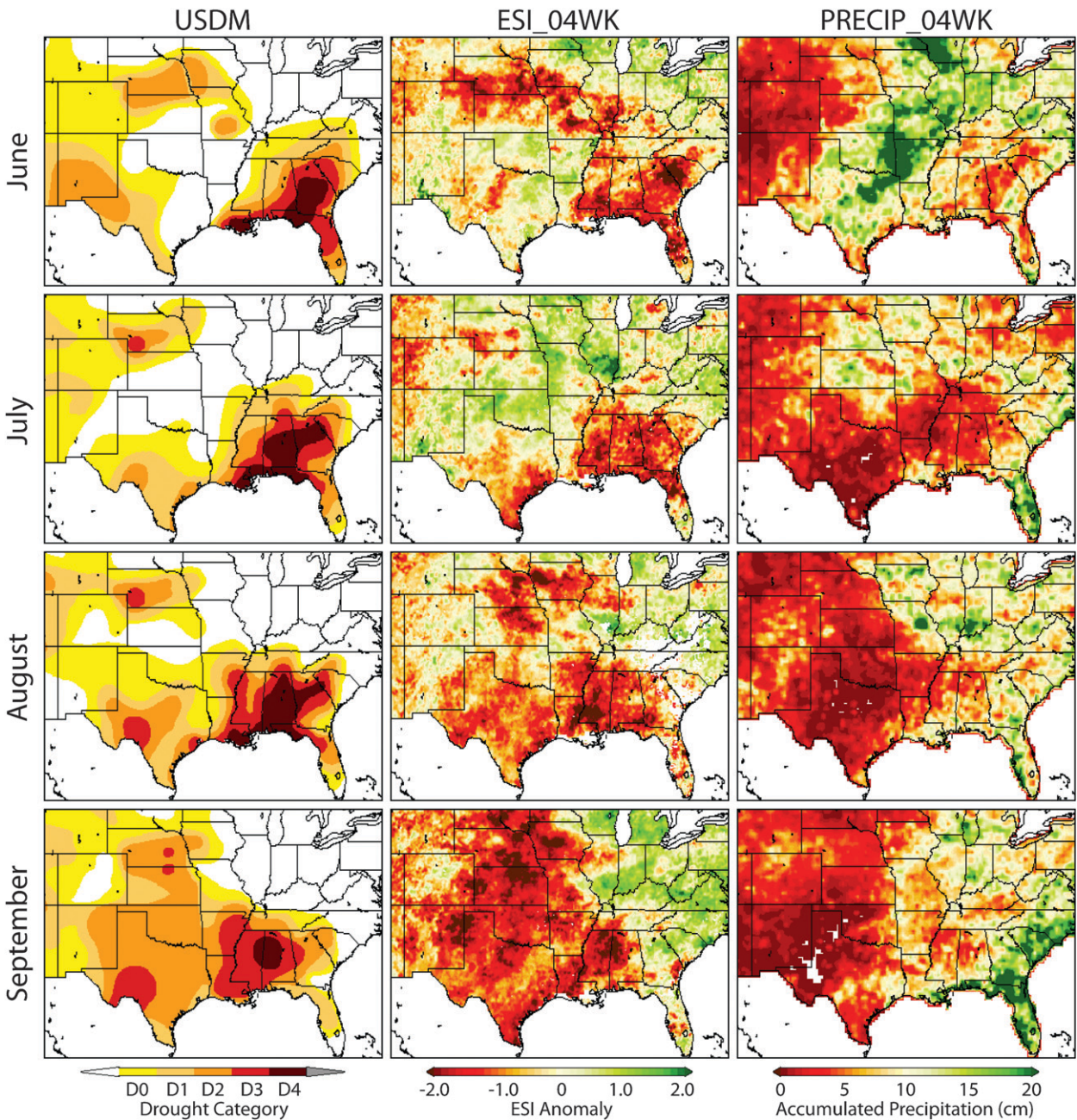


FIG. 2. Temporal evolution of the (left) USDM, (middle) 4-week ESI composite, and (right) 4-week accumulated precipitation (cm) from June to September 2000. Images are valid at the end of each month.

*b. USDM*

The USDM is a composite drought severity analysis created each week through expert synthesis of existing drought diagnostic metrics, rainfall and surface streamflow percentiles, crop conditions, and local impact reports from observers across the country (Svoboda et al. 2002). The goal of the USDM is to track and display the magnitude and spatial extent of drought and its impacts across

the United States by fusing disparate information from multiple data streams. It classifies drought severity into five categories, ranging from abnormally dry to exceptional drought, and distinguishes between short-term (i.e., agricultural drought) and long-term (i.e., hydrologic drought) impacts. Though it provides a useful analysis of current drought conditions, it should not be considered an absolute measure of drought severity because it is subjective and conveys information about

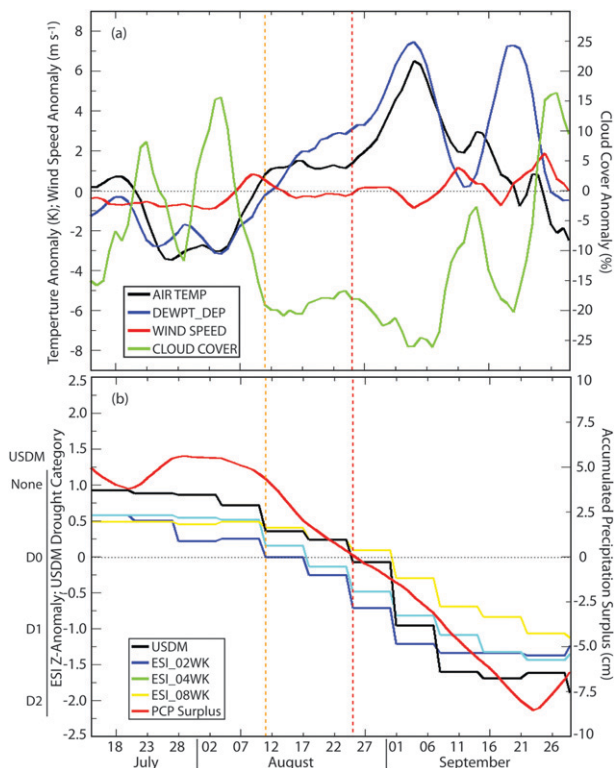


FIG. 3. (a) Time series of daily averaged 2-m air temperature (K), dewpoint depression (K), surface wind speed ( $\text{m s}^{-1}$ ), and cloud cover (%) anomalies for eastern Oklahoma and western Arkansas during 2000. (b) Time series of USDM drought category; ESI<sub>02WK</sub>, ESI<sub>04WK</sub>, and ESI<sub>08WK</sub> composites; and accumulated precipitation surplus (cm). The precipitation surplus is computed starting from 16 June. The vertical orange (red) dashed lines correspond to the first week in which at least one (four) of the 12  $\Delta$ ESI anomalies was below  $-1$ .

drought at multiple time scales and for a wide range of impacts (including socioeconomic impacts, which are not easily conveyed by other drought indicators). Indeed, an absolute measure of drought severity is difficult to obtain given the inherent complexity of the phenomenon. Still, comparisons with the USDM are useful for evaluating the capacity of the ESI to depict rapid onset drought events.

For this study, weekly USDM drought classification maps from 2000 to 2011 were provided by the National Drought Mitigation Center (NDMC) in shapefile format and then interpolated to the 10-km ALEXI CONUS grid. Numerical values were assigned to each drought category, with no drought set to  $-1$ , abnormally dry conditions (D0) at 0, moderate drought (D1) at 1, severe drought (D2) at 2, extreme drought (D3) at 3, and exceptional drought (D4) at 4.

### c. Crop condition data

The U.S. crop condition data for 2002–11 were provided by the USDA NASS. The dataset includes soil

moisture information along with estimates of the crop health status and phenological stage of major agricultural crops. Weekly surveys are conducted at the county level, collecting categorical assessments that are aggregated to state-level summaries published in the weekly NASS crop progress reports. The reported crop conditions range from very poor to excellent, where the latter indicates the potential for above-normal crop yields and the absence of water-related stress. For this study, numerical values were assigned to each crop condition category: very poor (0), poor (1), fair (2), good (3), and excellent (4). The weekly reports were averaged to monthly values for each county to account for gaps in the dataset. Because of the confidential nature of the dataset, the monthly county-level values were interpolated to the 10-km ALEXI grid and then spatially smoothed using a  $3 \times 3$  square moving window. Monthly crop condition anomalies were subsequently computed based on the 2002–11 mean conditions. In anomaly form, the impact of observer bias and normal seasonal cycles in crop condition is reduced, highlighting anomalous behavior at a given time and location. While these crop condition data are qualitative and categorical, when gridded they show good spatial coherence across counties and reasonable spatial correlation with patterns in the ESI and USDM maps, indicating value as an independent assessment of spatiotemporal drought impacts experienced by agricultural crops within the monitoring domain.

### d. Precipitation datasets

Accumulated precipitation across the CONUS was obtained from the Climate Prediction Center's unified gauge-based analysis of daily precipitation reports from cooperative observers and official National Weather Service reporting stations (Higgins et al. 2000). Daily precipitation amounts from the  $0.25^\circ$ -resolution grid were interpolated to the ALEXI domain and then summed to create 4-week rainfall totals used for spatial comparisons with the ESI and USDM. Time series of accumulated rainfall departures (surplus or deficit with respect to the climatology) were also computed for each flash drought event discussed in section 3. First, the average daily precipitation was computed over the 2000–11 time period. The observed daily precipitation was then subtracted from the mean. To account for the important role of antecedent precipitation, the accumulated surplus or deficit was then computed by summing these departures from a specified day several weeks before the start of a given drought event, which was defined as the first instance of a  $\Delta$ ESI anomaly less than  $-1$ .

It is important to note that ALEXI does not require precipitation data as input; it is used here simply as an independent dataset to evaluate the timing and

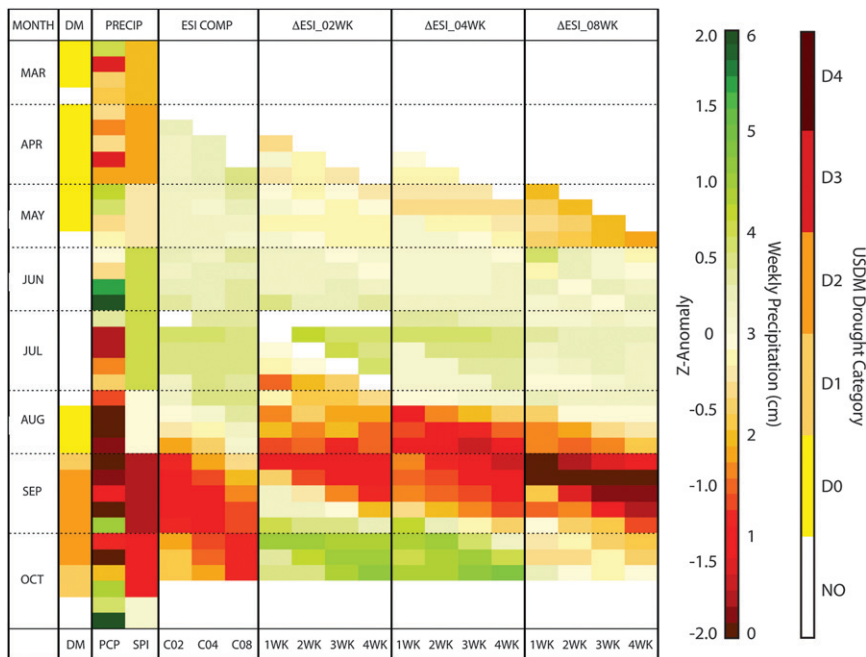


FIG. 4. Drought evolution across eastern Oklahoma and western Arkansas during 2000. The USDM drought category is shown in the first column with the accumulated precipitation (cm) and 3-month SPI anomaly shown in columns 2 and 3. ESI for 2-, 4-, and 8-week composite periods are shown in columns 4–6.  $\Delta$ ESI for 1-, 2-, 3-, and 4-week differencing intervals are shown in columns 7–10, 11–14, and 15–18 for the ESI 2-, 4-, and 8-week composite periods, respectively.

magnitude of rainfall departures. ESI data were also compared to the 3-month SPI (McKee et al. 1993, 1995) product, which is a standard drought monitoring tool computed using only precipitation observations. SPI data were available over CONUS on a 0.5°-resolution grid.

*e. NARR*

NARR (Mesinger et al. 2006) data were used to evaluate the atmospheric conditions present during the flash drought events. Daily averages were computed for cloud cover, 10-m wind speed, and 2-m temperature and dewpoint depression using analyses available every 3 h on a 32-km-resolution grid. A 7-day running mean was computed for each field to reduce short-term fluctuations, with smoothed daily anomalies calculated with respect to the 2000–11 daily mean values.

**3. Results**

This section examines the evolution of four flash drought events that occurred across the central United States during 2000–11 through a comparison of ESI, USDM, SPI, rainfall, and other surface meteorological data. The drought-affected areas studied here are

characterized by different vegetation types and agricultural practices, ranging from a mixture of pasture, range, and forest over eastern Oklahoma and western Arkansas to landscapes dominated by corn and soybeans in the Midwest (refer to Fig. 1). Each drought event varied in severity and duration and occurred during a different season. The NASS crop condition data (available after 2002) serve as a form of ground truth in evaluating the timing and severity of resulting impacts of these drought events on agricultural systems.

*a. Oklahoma and Arkansas: Late summer 2000*

The term “flash drought” was first used in 2000 to describe the rapid onset of severe drought conditions that occurred during late summer across portions of the southern United States. An overview of the large-scale environment within which the flash drought event occurred is provided in Fig. 2, which shows the USDM drought analysis at the end of each month from June to September along with 4-week ESI composites and monthly accumulated rainfall. Time series of meteorological variables (expressed as anomalies) considered important in driving rapid drought onset (clear skies, low rainfall, high winds, temperature, and dewpoint

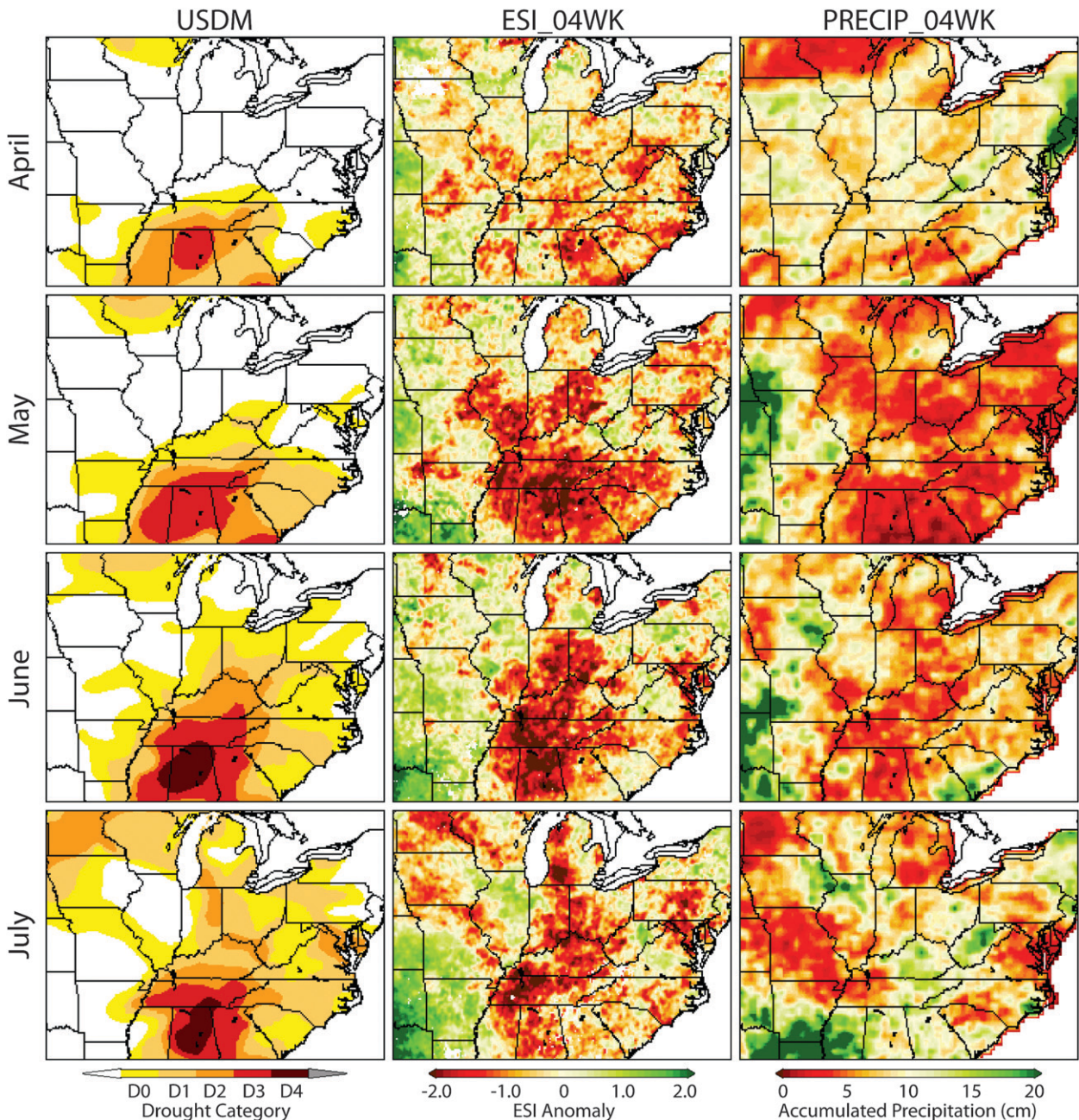


FIG. 5. As in Fig. 2, but from April to July 2007.

depression), averaged over eastern Oklahoma and western Arkansas (refer to Fig. 1), are shown in Fig. 3 along with the temporal response of the ESI and USDM drought indicators. Note that, following the sign convention used in many standard drought indicators, ESI becomes more negative as drought severity (and USDM drought class) increases.

At the end of June, several areas of severe drought were present within a band encircling the south-central

United States. Large negative ESI values had developed within these areas, suggesting that the abnormal dryness was limiting ET and adversely affecting the vegetation. Very heavy rainfall ( $>20$  cm) occurred in June over eastern Oklahoma and western Arkansas, where flash drought would develop several weeks later, leading to positive ESI across that region during July. Extremely dry weather persisted across much of the southern United States during July and August, causing expansion

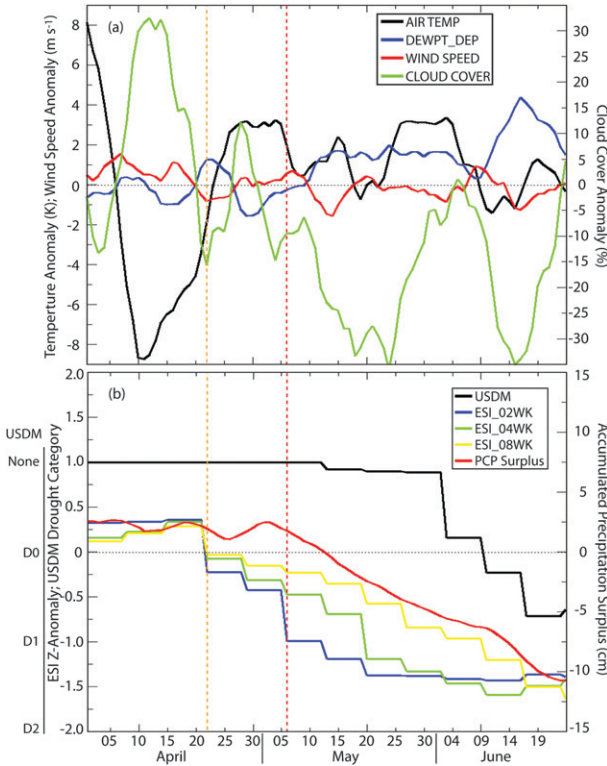


FIG. 6. As in Fig. 3, but for eastern Indiana and western Ohio during 2007. The precipitation surplus is computed starting from 18 March.

of drought conditions from Texas to Alabama. By the end of August, very warm temperatures combined with only light rainfall resulted in rapid decreases in ESI from Texas northward to Nebraska, with attendant increases in USDM drought coverage across the central United States. Drought intensification continued unabated for several more weeks, with large areas of Kansas, Oklahoma, and Arkansas experiencing up to a three-category increase in USDM-depicted drought intensity during September, which indicates how quickly severe drought conditions developed across the region.

To more closely examine the evolution of rapid-onset drought events, a new visualization method similar to a Hovmöller (1949) diagram was developed to synthesize drought information from multiple tools, including the USDM, SPI, observed rainfall, and the various time scales of ESI and  $\Delta$ ESI indicators discussed in section 2a. Figure 4 shows weekly values for each variable averaged over ALEXI grid points located in eastern Oklahoma and western Arkansas (refer to Fig. 1). The first three columns show USDM drought severity, weekly precipitation totals, and 3-month SPI. The following columns depict ESI and  $\Delta$ ESI time evolution, transitioning toward longer compositing and change intervals along

the horizontal axis. ESI values for 2-, 4-, and 8-week composites are shown in columns 4–6, while standardized change anomalies ( $\Delta$ ESI) in these composites computed over 1–4-week differencing intervals are shown in the following columns. White areas in the ESI and  $\Delta$ ESI columns denote missing data.

Rainfall during May and June over this region resulted in generally good vegetation health during the first half of summer, as inferred by the near-neutral ESI values and the absence of drought in the USDM. This was accompanied by negative air temperature, dewpoint depression, and wind speed anomalies (Fig. 3a) during July, indicating that atmospheric conditions were generally conducive to maintaining soil moisture reserves because of reduced ET demands.

By the end of July, however, conditions began to deteriorate because of limited rainfall across the area during preceding weeks. Though the ESI was still near average through the first two weeks of August, the appearance of large negative change anomalies indicated that ET was decreasing rapidly relative to the 12-yr climatology. The  $\Delta$ ESI first fell below  $-1\sigma$  on 12 August (indicated by the orange vertical line in Fig. 3). More substantial decreases in the ESI composites began during the last half of August and continued through most of September. This period was characterized by warmer temperatures and sunnier skies, which contributed to large increases in dewpoint depression because of the increased ET demands.

The unusual swiftness with which the ESI changes occurred is clearly depicted by the very large negative  $\Delta$ ESI values shown in the last 12 columns of Fig. 4. The largest negative ESI changes are first detected in the 1-week differencing interval data and then shift toward longer differencing intervals during subsequent weeks. This behavior results in a distinct “plume” of negative  $\Delta$ ESI in the visualization tool demonstrated in Fig. 4, which may prove to be a valuable early warning signal for rapid drought onset. The large negative change indicators were either coincident with the rapid introduction of severe drought in the USDM during the first two weeks of September or led the USDM by several weeks depending on which composite and differencing interval was used. The stress signature conveyed by the normalized ESI change indicators also preceded a notable signal in the ESI itself, which appears in Fig. 3 to closely track the increase in USDM drought severity. Beneficial rainfall during the last week of September led to some improvements in the ESI and the return of positive  $\Delta$ ESI values. Still, the USDM drought depiction remained unchanged for several more weeks because of the long-term hydrological impacts of the severe drought.

*b. Indiana and Ohio: Early summer 2007*

This section examines a flash drought event that occurred across eastern Indiana and western Ohio during early summer 2007. This region is characterized by extensive areas of corn and soybean production. Inspection of Fig. 5 shows that the region was drought-free during the spring; however, severe drought over the southeastern United States rapidly expanded northward in June and July. Heavy rainfall (8–12 cm) in April was accompanied by a prolonged period of cooler than normal temperatures (Fig. 6) that delayed crop emergence. Scattered areas of negative ESI across the region suggest that crop water use was less than normal, likely because of phenological delays. Local crop reports stated that the dry weather during May allowed farmers to rapidly plant their remaining crop acreage so that planting was ahead of schedule by the end of the month, with the average corn and soybean growth stages returning to normal for that time of year (USDA 2007). The very dry weather that aided planting, however, also led to increased moisture stress and large negative ESI values in May, presumably because the immature plants were unable to access moisture below the root zone. Below normal rainfall persisted during June and July, coincident with the introduction of moderate to severe drought conditions in the USDM and a deterioration in average crop conditions, particularly in rangeland and pasture (Fig. 7).

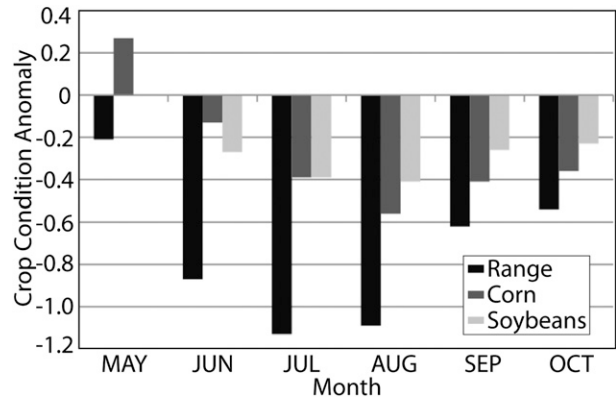


FIG. 7. Monthly crop condition anomalies for eastern Indiana and western Ohio during 2007.

Figure 8 depicts drought onset using the ESI and  $\Delta$ ESI visualization tool, computed as an average of ALEXI grid points located within the three easternmost climate divisions of Indiana and the three westernmost divisions of Ohio. Overall, conditions were near normal at the beginning of April but started to deteriorate thereafter. The initial appearance of large negative  $\Delta$ ESI ( $> -1\sigma$ ) at the end of April (orange vertical line in Fig. 6) likely represents reductions in ET due to delayed vegetation growth rather than incipient water stress. Though not related to drought, this information is still potentially useful within the agricultural sector because it provides

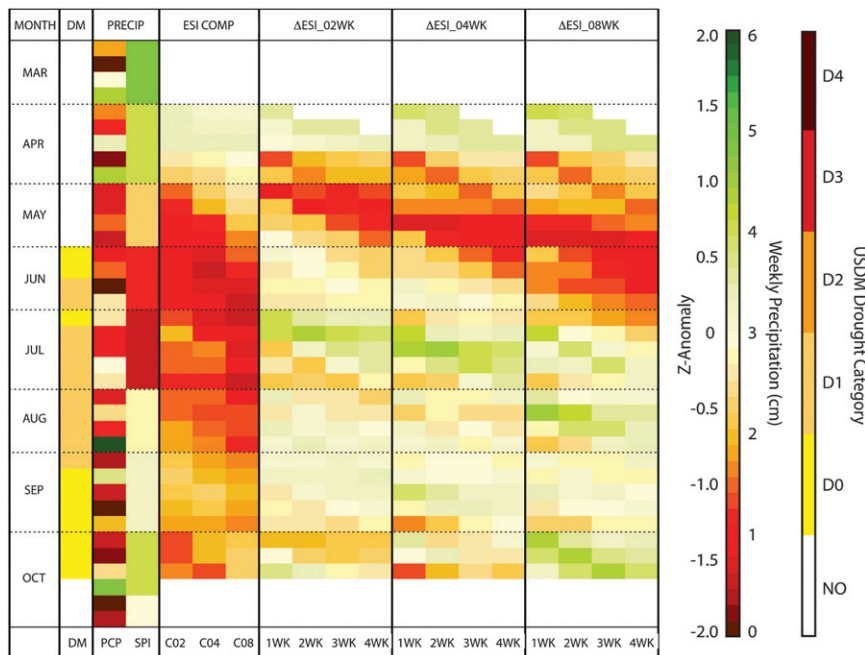


FIG. 8. As in Fig. 4, but for eastern Indiana and western Ohio during 2007.

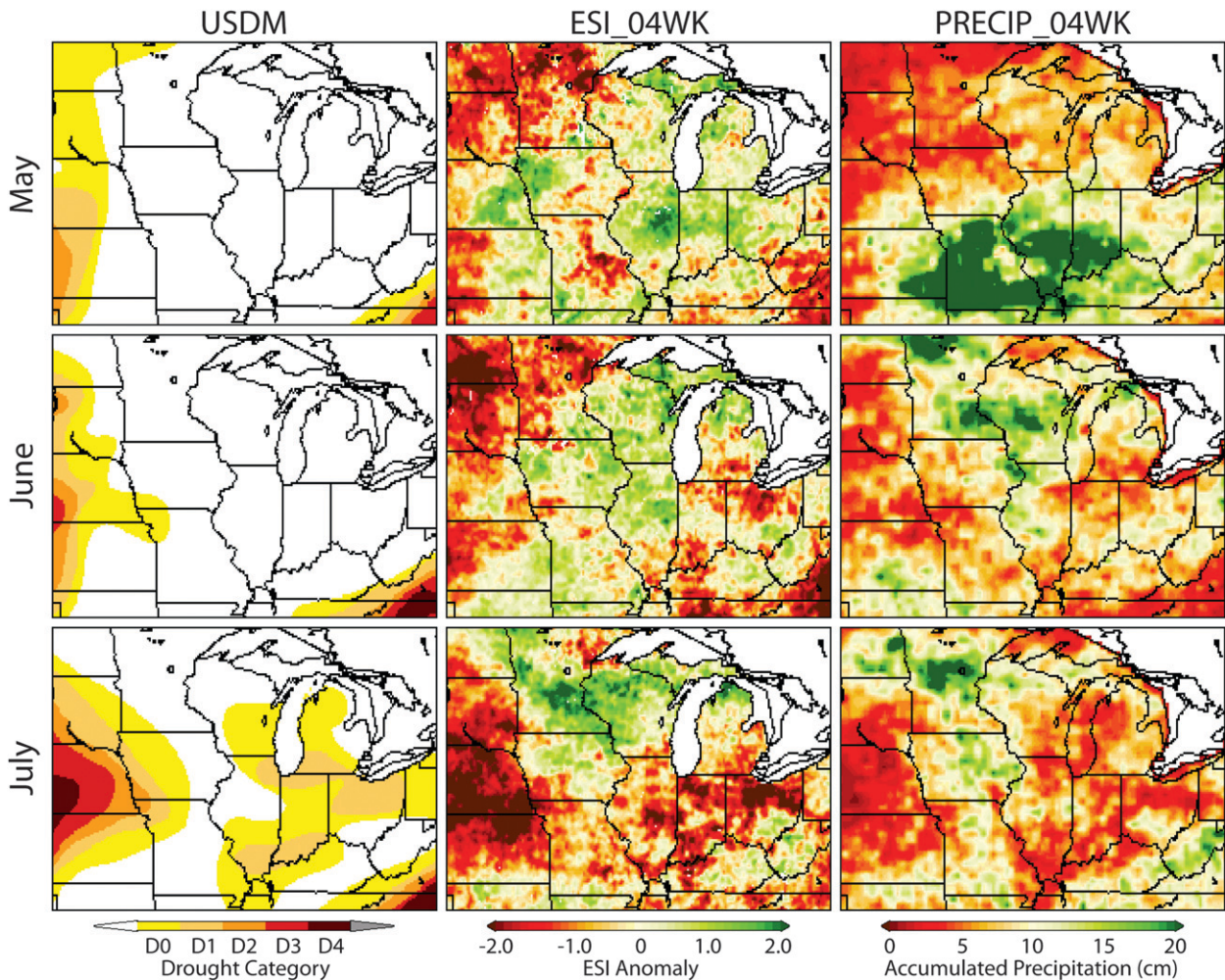


FIG. 9. As in Fig. 2, but from May to July 2002.

additional evidence that crops may be growing slower than normal.

An almost complete lack of rainfall during May led to a rapid decrease in all  $\Delta$ ESI products, appearing first in the 2-week  $\Delta$ ESI composites and then cascading to the longer composite periods during later weeks. This was accompanied by warmer conditions that developed across the region by the end of the month and persisted through the middle of June, along with increased solar insolation due to predominantly clear skies (Fig. 6). Although winds were near normal during this event, the abnormally warm and cloud-free conditions led to higher dewpoint depressions along with increased ET and soil moisture depletion. The USDM began to indicate abnormal dryness and then moderate drought conditions by the middle of June, several weeks after all of the  $\Delta$ ESI indicators first indicated that vegetation and moisture conditions were not normal. Early warning of the degradation in crop conditions in June (Fig. 7) may have

been conveyed by the negative  $\Delta$ ESI plume signal in early May. Conditions of all crop types improved in September because of increasing rainfall starting in late August, as evidenced in weakly positive  $\Delta$ ESI.

### c. Southeast Wisconsin: Summer 2002

In contrast to the several-month drought described in section 3b, this section describes the evolution of a short-duration flash drought event that occurred across southeastern Wisconsin during summer 2002. This region is generally characterized by gently rolling terrain dominated by farmland and several large urban areas. Figure 9 shows the USDM drought depiction, 4-week ESI composites, and total accumulated rainfall at the end of each month from May until July. Time series of average meteorological conditions computed over ALEXI grid points located within the southeastern Wisconsin climate division (refer to Fig. 1) are shown in Fig. 10.

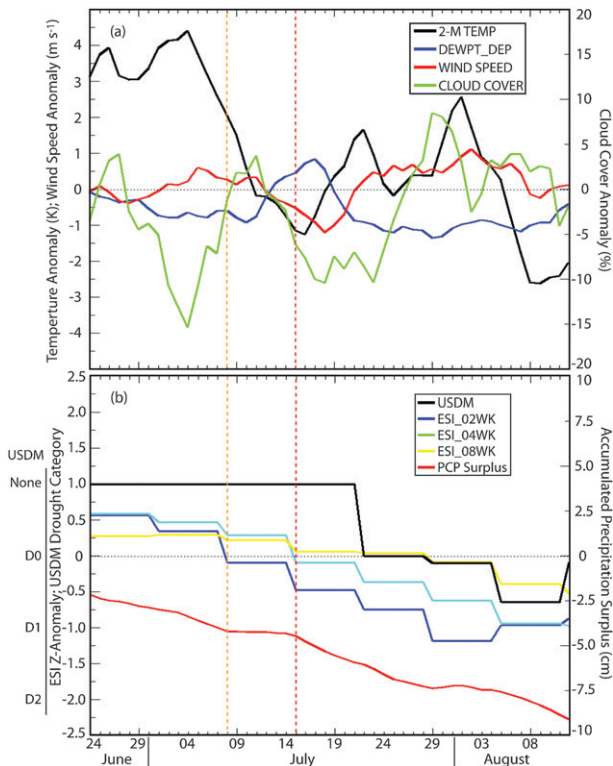


FIG. 10. As in Fig. 3, but for southeastern Wisconsin during 2002. The precipitation surplus is computed starting from 10 June.

After receiving nearly normal precipitation during late winter and early spring (not shown), drier weather prevailed across the upper Midwest during May, with a band of heavy precipitation occurring further to the south from Missouri eastward into southern Indiana. While the USDM indicated that drought conditions were not present at this time, scattered areas of negative ESI suggest that the vegetation was beginning to show early signs of water stress in some locations. While rainfall amounts were low across most of the region during June, beneficial rain across portions of Minnesota and Wisconsin contributed to more favorable growing conditions as implied by generally positive values of ESI. Additional heavy rainfall during July maintained high ET rates across Minnesota, northern Iowa, and western Wisconsin, but areas to the south and east received much less precipitation, which combined with above normal temperatures (Fig. 10) to drive the rapid development of large negative ESI and the introduction of drought conditions in the USDM by the end of July. The switch from positive to negative ESI during July was due not only to the increasing rainfall deficit and its effect on surface moisture but also to the increased evaporative demand associated with the warmer conditions and

strong radiative forcing due to predominantly clear skies. Unlike the previous case studies, in this event the dewpoint depression anomalies did not increase during the drought even though daily ET values had declined. Closer inspection of daily weather maps (not shown) revealed that the smaller dewpoint depressions were due to a combination of persistent northerly winds transporting moisture from nondrought areas and the more frequent occurrence of lake breezes moving far inland from Lake Michigan during the afternoon and evening. Both of these processes helped offset local decreases in lower tropospheric water vapor caused by the anomalously low ET rates.

The associated  $\Delta$ ESI visualization for this event is shown in Fig. 11. Overall, growing conditions were favorable during the first half of summer, as indicated by the generally positive ESI. The appearance of a weak negative  $\Delta$ ESI plume in May, however, indicates that conditions were beginning to deteriorate before increased precipitation during the first three weeks of June temporarily halted drought development. An extended period of extremely dry weather subsequently began at the end of June and lasted until the middle of August, impacting crop conditions reported by NASS for pasture, corn, and soybeans in these months (Fig. 12). Though the ESI composites remained near normal until the middle of July, the appearance of large  $\Delta$ ESI anomalies provided early evidence that plant available water was decreasing rapidly. Abnormal dryness was first indicated by the USDM two weeks after the initial occurrence of large negative change anomalies in the 2-week ESI composites (Fig. 10). Drought conditions continued to intensify through the first half of August before very heavy rainfall at the end of the month alleviated the drought as classified in the USDM (Fig. 11) and resulted in improved crop condition, reflected in the NASS dataset (Fig. 12). The rapid increase in ET following the heavy rainfall is indicated by the plume of positive  $\Delta$ ESI anomalies that preceded the return of much above normal ESI values during September. Though short lived, the timing of the flash drought event during the crop pollination and grain filling stages resulted in a lasting negative impact on crop conditions, especially for corn, which is a very important feed source for local dairy farmers.

#### d. Oklahoma and Arkansas: Summer 2011

A recent flash drought event that occurred across eastern Oklahoma and western Arkansas during the summer of 2011 is described in this section. Figure 13 shows the USDM drought depiction, ESI\_04WK composites, and total monthly rainfall across the south-central United States at the end of each month from

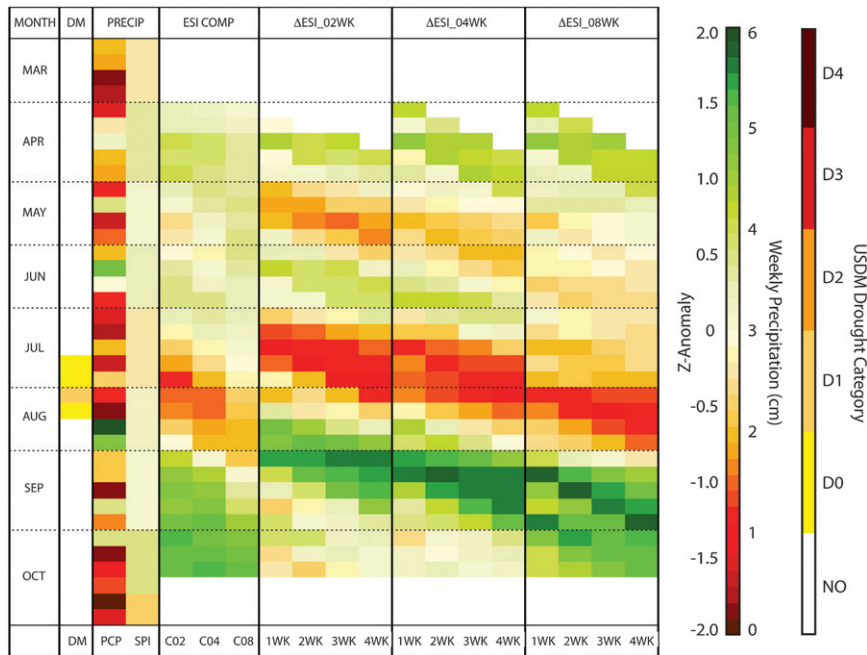


FIG. 11. As in Fig. 4, but for southeastern Wisconsin during 2002.

April until July, with time series of average surface meteorological anomalies for eastern Oklahoma and western Arkansas shown in Fig. 14. After receiving below-normal precipitation during the winter (see 3-month SPI in Fig. 16), widespread drought conditions were observed across a large portion of the south-central United States at the beginning of spring (not shown). Rainfall was highly variable across the region during April and May, with some areas receiving copious amounts of rainfall, whereas others remained drier than normal, especially along the Gulf Coast and in western Texas. Several episodes of intense, persistent thunderstorm activity produced extremely heavy rainfall across a broad region extending from eastern Oklahoma to the Ohio River Valley, eliminating drought conditions from those areas. Patterns in ESI show good correspondence with USDM classifications during this time period.

By the beginning of June, much warmer and sunnier conditions quickly developed across the region and persisted almost without interruption until the end of summer (Fig. 14). Anomalously high evaporation rates were further augmented by unusually strong wind speeds that quickly depleted surface moisture and contributed to the development of large positive dewpoint depression anomalies. Very little rainfall during June allowed drought conditions to intensify in Texas and along the Gulf Coast, with northward expansion of abnormal dryness into eastern Oklahoma and most of Arkansas (Fig. 13). The USDM drought depiction

indicates that rapid drought intensification occurred during July, with some locations experiencing up to a three-category increase in drought severity. Extensive areas with strongly negative ESI values ( $< -1\sigma$ ) indicate that the vegetation health was very poor, as the plants were unable to adequately respond to the extreme conditions. This depiction is supported by the below-average pasture and range conditions in June and their rapid deterioration in July (Fig. 15).

The corresponding  $\Delta$ ESI visualization tool for this event is shown in Fig. 16. After a brief respite from drought conditions during May, abnormal dryness was reintroduced in the USDM by the end of June. The  $\Delta$ ESI

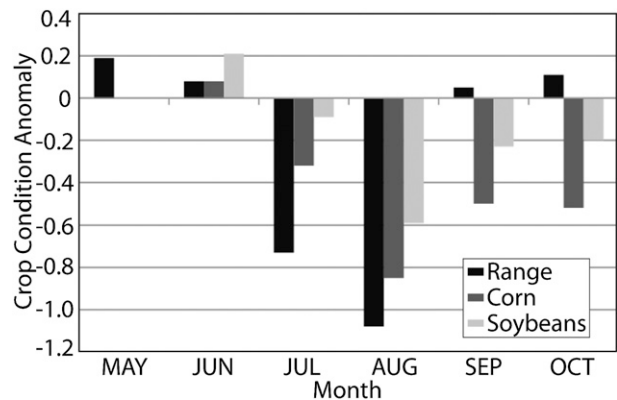


FIG. 12. Monthly crop condition anomalies for southeastern Wisconsin during 2002.

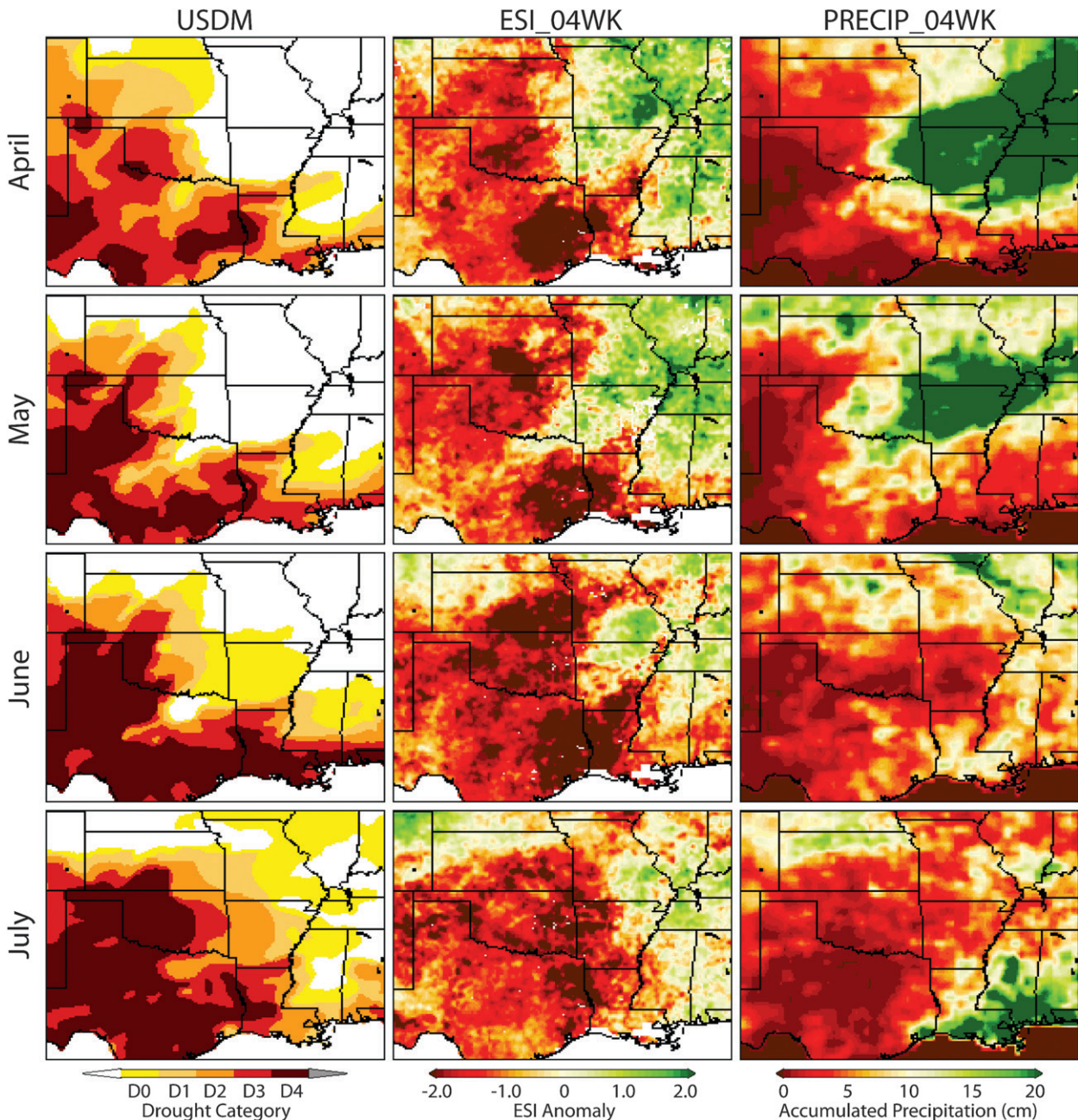


FIG. 13. As in Fig. 2, but from June to September 2011.

indicators show that conditions were already beginning to deteriorate across the region at the end of May despite receiving very heavy rainfall during the previous six weeks. The first change anomaly less than  $-1\sigma$  occurred on 10 June, with all change indicators becoming strongly negative the following week. In response to the persistent elevated surface temperatures and lack of rainfall (Fig. 14), rapid deterioration continued for two additional months with all of the change indicators

remaining negative until the end of July. The longevity of the large negative change anomalies is impressive considering that the ESI composites were already well below zero by the end of June. Comparison with the 3-month SPI in Fig. 16 and the shorter-term rainfall deficit in Fig. 14 shows that the  $\Delta$ ESI anomalies provided much earlier warning that severe drought conditions were rapidly developing across the region. These results suggest that reliance on precipitation-based

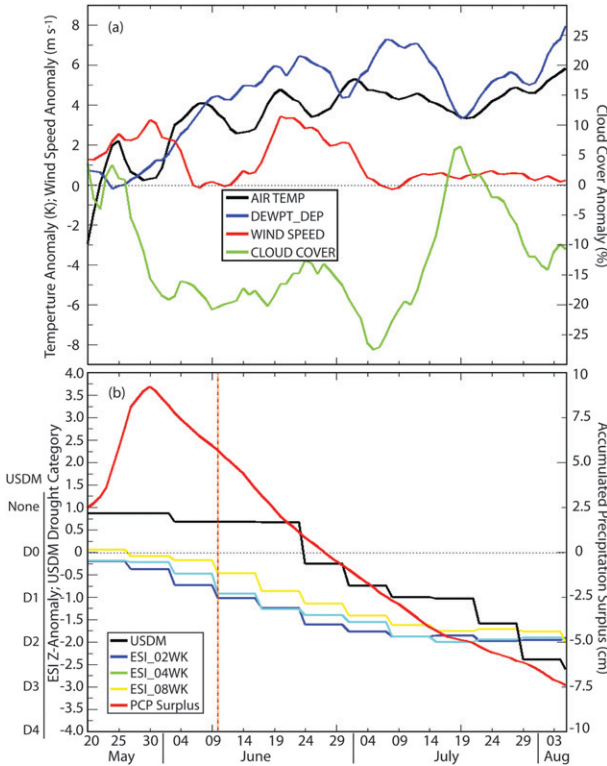


FIG. 14. As in Fig. 3, but for eastern Oklahoma and western Arkansas during 2011. The precipitation surplus is computed starting from 29 April.

drought metrics alone to determine drought severity can be misleading in situations characterized by large temperature, radiation, and wind anomalies. For example, the drought severity in the USDM increased much more slowly than was suggested by the ESI and  $\Delta$ ESI, with the introduction of severe drought lagging the ESI by up to a month.

**4. Conclusions**

This study examined the evolution of several flash drought events that impacted different areas of the United States in recent years through a comparison of surface meteorological data, USDM drought analyses, and ET anomalies inferred by the TIR-based ESI. Each drought event varied in severity and duration and occurred during different parts of the growing season. Affected areas were characterized by diverse primary vegetation types ranging from forest and grass over eastern Oklahoma and western Arkansas to intensive corn and soybean production over the Midwestern Corn Belt. To more easily evaluate anomalous ET conditions across different seasons and regions, standardized  $z$  anomalies were computed each week for 2-, 4-, and

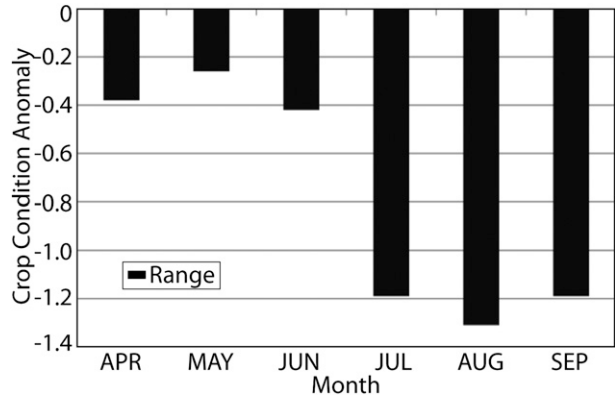


FIG. 15. Monthly range/pasture condition anomalies for eastern Oklahoma and western Arkansas during 2011.

8-week composite periods based on the average conditions experienced during the ALEXI period of record (2000–11). Standardized change anomalies computed for 1-, 2-, 3-, and 4-week change intervals for each ESI composite product allow evaluation of information content in the first derivative of the temporal stress signal.

Examination of meteorological time series identified characteristic behaviors associated with these rapid onset events. All were associated with positive temperature anomalies and low cloud cover, while the most severe cases also exhibited persistently high winds and dewpoint depressions, serving to enhance rapid evaporative depletion of soil moisture reserves. In each of these case studies the change anomalies conveyed useful information about the rate at which vegetation health and plant available water were deteriorating and provided early warning of incipient impacts on crop condition, as indicated by ground observations collected by NASS. Large negative change anomalies indicative of rapidly drying conditions initially developed in the 1-week differencing interval data for each composite period before shifting toward longer differencing intervals during subsequent weeks. This behavior combined with the tendency for large negative change anomalies to first appear in the shorter composite data contributed to the development of downward sloping “plumes” of negative anomalies in the weekly ESI change images. Inspection of other flash drought cases not shown in this paper revealed that this is a common feature associated with rapid drought onset. The large negative change anomalies were either coincident with the rapid introduction of drought conditions by the USDM or led the USDM drought depiction by several weeks, depending on the composite and time differencing interval. The shortest composite and differencing intervals typically provided the earliest warning of impending drought

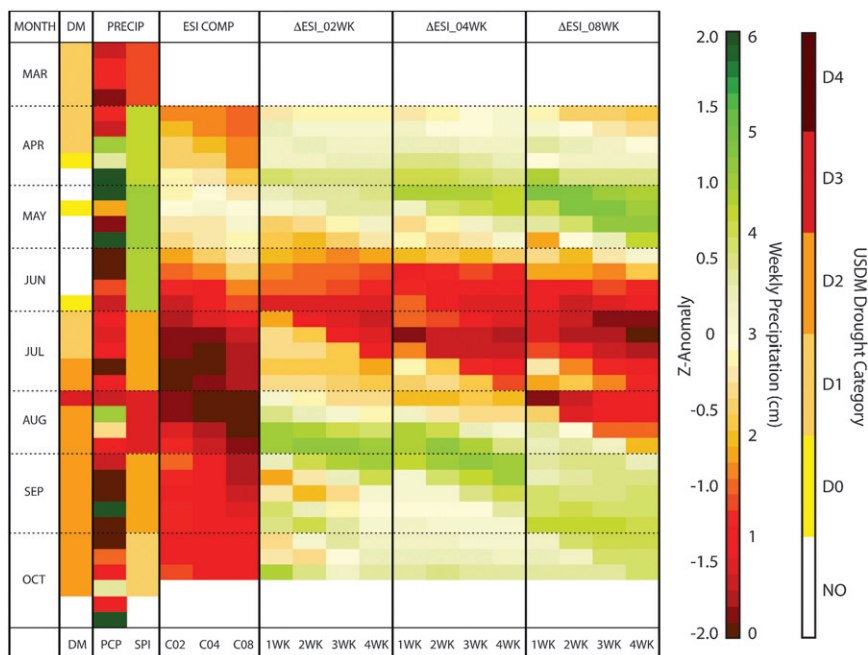


FIG. 16. As in Fig. 4, but for eastern Oklahoma and western Arkansas during 2011.

intensification because they respond more quickly to rapidly changing conditions.

Taken together, these results demonstrate that drought indicators based on remotely sensed TIR observations can improve the effectiveness of drought early warning systems because large decreases in ET often precede both the occurrence of large rainfall deficits and reductions in vegetation biomass during early stages of drought development. Unlike drought indices derived from in situ precipitation observations or radar-derived precipitation estimates, the ESI, which does not rely on any observations of antecedent precipitation, can be readily adapted for use in data-sparse regions, making it well suited for monitoring drought conditions at global scales. Furthermore, drought indicators based on water demand (i.e., ET) may have particular utility for assessing agricultural drought because even short periods of drought can result in substantial yield losses and poor grain quality if the water-related stress occurs during a sensitive stage of crop development.

Ongoing studies are quantitatively examining the robustness of negative ESI change anomalies as an early drought indicator. Analyses of correlation between the magnitude and duration of the negative change anomaly plumes and subsequent increases in USDM drought severity are being used to quantify the frequency with which drought is correctly identified. Evaluation of spatiotemporal correlations of ESI and  $\Delta$ ESI with gridded NASS crop condition, soil moisture, and yield data will

provide a means to quantify early warning potential in the remotely sensed ESI stress signals in comparison with impacts observed in the field and in comparison with other indicators of agricultural drought. Other studies will use high-resolution soil, vegetation, and atmospheric data to quantify the role of vegetation in driving flash drought development. Finally, potential for integration of the ESI and ESI change products into the USDM construction process is being investigated in collaboration with USDM authors, with the goal of enhancing response capability during rapidly evolving drought events.

*Acknowledgments.* This work was supported by funds provided by the NOAA Climate Program Office under Grant GC09-236. Special thanks are given to Brad Pierce (NOAA/ASPB) and Sharon Nebuda (CIMSS) for their IDL programming assistance. Comments from three anonymous reviewers improved the manuscript.

## REFERENCES

- Allen, R. G., L. S. Pereira, D. Raes, and M. Smith, 1998: Crop evapotranspiration: Guidelines for computing crop water requirements. FAO Irrigation and Drainage Paper 56, FAO, Rome, 328 pp.
- Anderson, M. C., J. M. Norman, G. R. Diak, W. P. Kustas, and J. R. Mecikalski, 1997: A two-source time-integrated model for estimating surface fluxes using thermal infrared remote sensing. *Remote Sens. Environ.*, **60**, 195–216.

- , W. P. Kustas, and J. M. Norman, 2007a: Upscaling flux observations from local to continental scales using thermal remote sensing. *Agron. J.*, **99**, 240–254.
- , J. M. Norman, J. R. Mecikalski, J. A. Otkin, and W. P. Kustas, 2007b: A climatological study of evapotranspiration and moisture stress across the continental United States based on thermal remote sensing: 1. Model formulation. *J. Geophys. Res.*, **112**, D10117, doi:10.1029/2006JD007506.
- , —, —, —, and —, 2007c: A climatological study of evapotranspiration and moisture stress across the continental United States based on thermal remote sensing: 2. Surface moisture climatology. *J. Geophys. Res.*, **112**, D11112, doi:10.1029/2006JD007507.
- , C. Hain, B. Wardlow, A. Pimstein, J. R. Mecikalski, and W. P. Kustas, 2011: Evaluation of drought indices based on thermal remote sensing and evapotranspiration over the continental United States. *J. Climate*, **24**, 2025–2044.
- , and Coauthors, 2012: Mapping daily evapotranspiration at Landsat spatial scales during the BEAREX'08 field campaign. *Adv. Water Resour.*, **50**, 162–177.
- , W. P. Kustas, J. A. Otkin, X. Zhan, K. Mo, M. Svoboda, B. Wardlow, and A. Pimstein, 2013: An intercomparison of drought indicators based on thermal remote sensing and NLDAS simulations. *J. Hydrometeorol.*, in press.
- Barnabás, B., K. Jäger, and A. Fehér, 2008: The effect of drought and heat stress on reproductive processes in cereals. *Plant Cell Environ.*, **31**, 11–38.
- Brown, J. F., B. D. Wardlow, T. Tadesse, M. J. Hayes, and B. C. Reed, 2008: The Vegetation Drought Response Index (VegDRI): A new integrated approach for monitoring drought stress in vegetation. *GISci. Remote Sens.*, **45**, 16–46.
- Ciais, P., and Coauthors, 2005: Europe-wide reduction in primary productivity caused by heat and drought in 2003. *Nature*, **437**, 529–533.
- Higgins, R. W., W. Shi, E. Yarosh, and R. Joyce, 2000: Improved United States precipitation quality control system and analysis. NCEP/Climate Prediction Center ATLAS 7, Camp Springs, MD, 40 pp.
- Hovmöller, E., 1949: The trough-and-ridge diagram. *Tellus*, **1**, 62–66.
- Hu, A., and G. D. Willson, 2000: Effects of temperature anomalies on the Palmer Drought Severity Index in the central United States. *Int. J. Climatol.*, **20**, 1899–1911.
- Jiang, Y., and B. Huang, 2001: Drought and heat stress injury to two cool season turf grasses in relation to antioxidant metabolism and lipid peroxidation. *Crop Sci.*, **41**, 436–442.
- Karl, T. R., 1986: The sensitivity of the Palmer Drought Severity Index and Palmer's Z-Index to their calibration coefficients including potential evapotranspiration. *J. Climate Appl. Meteorol.*, **25**, 77–86.
- Kebede, H., D. K. Fisher, and L. D. Young, 2012: Determination of moisture deficit and heat stress tolerance in corn using physiological measurements and a low-cost microcontroller-based monitoring system. *J. Agron. Crop Sci.*, **198**, 118–129.
- Kogan, F. N., 1997: Global drought watch from space. *Bull. Amer. Meteor. Soc.*, **78**, 621–636.
- Li, Y. P., W. Ye, M. Wang, and X. D. Yan, 2009: Climate change and drought: A risk assessment of crop-yield impacts. *Climate Res.*, **39**, 31–46.
- McKee, T. B., N. J. Doesken, and J. Kleist, 1993: The relationship of drought frequency and duration to time scale. Preprints, *Eighth Conf. on Applied Climatology*, Boston, MA, Amer. Meteor. Soc., 179–184.
- , —, and —, 1995: Drought monitoring with multiple time scales. Preprints, *Ninth Conf. on Applied Climatology*, Anaheim, CA, Amer. Meteor. Soc., 233–236.
- McNaughton, K. G., and T. W. Spriggs, 1986: A mixed-layer model for regional evaporation. *Bound.-Layer Meteorol.*, **74**, 262–288.
- Mecikalski, J. M., G. R. Diak, M. C. Anderson, and J. M. Norman, 1999: Estimating fluxes on continental scales using remotely sensed data in an atmospheric–land exchange model. *J. Appl. Meteorol.*, **38**, 1352–1369.
- Mesinger, F., and Coauthors, 2006: North American Regional Reanalysis. *Bull. Amer. Meteor. Soc.*, **87**, 343–360.
- Mishra, V., and K. Cherkauer, 2010: Retrospective droughts in the crop growing season: Implications to corn and soybean yield in the Midwestern United States. *Agric. For. Meteorol.*, **150**, 1030–1045.
- Mittler, R., 2006: Abiotic stress, the field environment and stress combination. *Trends Plant Sci.*, **11**, 15–19.
- Mkhabela, M., P. Bullock, M. Gervais, G. Finlay, and H. Sapirstein, 2010: Assessing indicators of agricultural drought impacts on spring wheat yield and quality on the Canadian prairies. *Agric. For. Meteorol.*, **150**, 399–410.
- Moran, M. S., 2003: Thermal infrared measurement as an indicator of plant ecosystem health. *Thermal Remote Sensing in Land Surface Processes*, D. A. Quattrochi and J. Luvall, Eds., Taylor and Francis, 257–282.
- Mozny, M., M. Trnka, Z. Zalud, P. Hlavinka, J. Nekovar, V. Potop, and M. Virag, 2012: Use of a soil moisture network for drought monitoring in the Czech Republic. *Theor. Appl. Climatol.*, **107**, 99–111.
- Myneni, R. B., and Coauthors, 2002: Global products of vegetation leaf area and fraction absorbed by PAR from year of MODIS data. *Remote Sens. Environ.*, **83**, 214–231.
- Norman, J. M., W. P. Kustas, and K. S. Humes, 1995: A two-source approach for estimating soil and vegetation energy fluxes from observations of directional radiometric surface temperature. *Agric. For. Meteorol.*, **77**, 263–292.
- Otkin, J. A., M. C. Anderson, J. R. Mecikalski, and G. R. Diak, 2005: Validation of GOES-based insolation estimates using data from the United States Climate Reference Network. *J. Hydrometeorol.*, **6**, 460–475.
- Palmer, W. C., 1965: Meteorological drought. U.S. Weather Bureau Research Paper 45, NOAA, Silver Spring, MD, 58 pp.
- Pradhan, G. P., P. V. V. Prasad, A. K. Fritz, M. B. Kirkham, and B. S. Gill, 2012: Response of *Aegilops* species to drought stress during reproductive stages of development. *Funct. Plant Biol.*, **39**, 51–59.
- Prasad, P. V. V., S. R. Pisipati, I. Momcilovic, and Z. Ristic, 2011: Independent and combined effects of high temperature and drought stress during grain filling on plant yield and chloroplast EF-Tu expression in spring wheat. *J. Agron. Crop Sci.*, **197**, 430–441.
- Rizhsky, L., H. Liang, and R. Mittler, 2002: The combined effect of drought stress and heat shock on gene expression in tobacco. *Plant Physiol.*, **130**, 1143–1151.
- Rötter, R., and S. C. van de Geijn, 1999: Climate change effects on plant growth, crop yield, and livestock. *Climate Change*, **43**, 651–681.
- Saini, H. S., and M. E. Westgate, 1999: Reproductive development in grain crops during drought. *Adv. Agron.*, **68**, 59–96.
- Svoboda, M., and Coauthors, 2002: The drought monitor. *Bull. Amer. Meteor. Soc.*, **83**, 1181–1190.

- Swain, S., B. D. Wardlow, S. Narumalani, T. Tadesse, and K. Callahan, 2011: Assessment of vegetation response to drought in Nebraska using Terra–MODIS land surface temperature and Normalized Difference Vegetation Index. *GISci. Remote Sens.*, **48**, 432–455.
- USDA, 2007: *Weekly Weather and Crop Bulletin*. Vol. 94, No. 22, USDA, Washington, DC, 32 pp. [Available online at [http://usda01.library.cornell.edu/usda/waob/weather\\_weekly/2000s/2007/weather\\_weekly-05-31-2007.pdf](http://usda01.library.cornell.edu/usda/waob/weather_weekly/2000s/2007/weather_weekly-05-31-2007.pdf).]
- Xia, Y., M. B. Ek, H. Wei, and J. Meng, 2012a: Comparative analysis of relationships between NLDAS-2 forcings and model outputs. *Hydrol. Processes*, **26**, 467–474.
- , and Coauthors, 2012b: Continental-scale water and energy flux analysis and validation of the North American Land Data Assimilation System project phase 2 (NLDAS-2): 1. Intercomparison and application of model products. *J. Geophys. Res.*, **117**, D03109, doi:10.1029/2011JD016048.